JGP Journal of General Physiology

RESEARCH ARTICLE

# Epilepsy-associated mutations in the voltage sensor of KCNQ3 affect voltage dependence of channel opening

Rene Barro-Soria

**One of the major factors known to cause neuronal hyperexcitability is malfunction of the potassium channels formed by KCNQ2 and KCNQ3. These channel subunits underlie the M current, which regulates neuronal excitability. Here, I investigate the molecular mechanisms by which epilepsy-associated mutations in the voltage sensor (S4) of KCNQ3 cause channel malfunction. Voltage clamp fluorometry reveals that the R230C mutation in KCNQ3 allows S4 movement but shifts the open/closed transition of the gate to very negative potentials. This results in the mutated channel remaining open throughout the physiological voltage range. Substitution of R230 with natural and unnatural amino acids indicates that the functional effect of the arginine residue at position 230 depends on both its positive charge and the size of its side chain. I find that KCNQ3-R230C is hard to close, but it is capable of being closed at strong negative voltages. I suggest that compounds that shift the voltage dependence of S4 activation to more positive potentials would promote gate closure and thus have therapeutic potential.**

## Introduction

Voltage-gated $K^+$ channels (Kv) regulate and modulate the resting potential and set the threshold and duration of the action potential in excitable cells. One of the major potassium currents in neurons is the muscarine-regulated M current ($I_{KM}$), a noninactivating current with slow activation and deactivation kinetics and a negative voltage for half-activation ($V_{1/2}$; approximately −60 mV; Brown and Adams, 1980; Halliwell and Adams, 1982). The $I_{KM}$ current is primarily conducted by heterotetramers of KCNQ2 and KCNQ3 α-subunits (Wang et al., 1998), which are expressed in the central and peripheral nervous system (Brown and Adams, 1980; Halliwell and Adams, 1982). The biophysical properties combined with the specific subcellular localization allows $I_{KM}$ to regulate the membrane resting potential and depress repetitive neuronal firing (Brown and Adams, 1980). Mutations in neuronal KCNQ channels are associated with hyperexcitability-related disorders, including neuropathic pain (Jentsch, 2000; Maljevic and Lerche, 2014), benign familial neonatal seizures (Biervert et al., 1998; Charlier et al., 1998; Singh et al., 1998), and neonatal epileptic encephalopathy (Rauch et al., 2012; Saitsu et al., 2012; Weckhuysen et al., 2012, 2013; Kato et al., 2013; Orhan et al., 2014). However, how variants in the neuronal KCNQ channels contribute to the severity of disease and the molecular mechanisms underlying mutated-channel defects remains largely unknown.

KCNQ channels belong to the superfamily of Kv channels, which are tetrameric proteins with six transmembrane segments (S1–S6) per subunit (Fig. 1 A). In Kv channels, S5–S6 of the four subunits together form a centrally located pore that is flanked by the four voltage-sensing domains, each composed of S1–S4 (Long et al., 2005). The C-terminal end of the S6 segments form the gate (del Camino and Yellen, 2001; Sun and MacKinnon, 2017), and the fourth TM segment (S4) functions as the voltage sensor (Aggarwal and MacKinnon, 1996; Larsson et al., 1996; Mannuzzu et al., 1996; Seoh et al., 1996; Yang et al., 1996; Osteen et al., 2010). At rest, S4 is assumed to be in its inward state and, in response to depolarization, moves outward, thereby opening the channel gate to allow $K^+$ flow (Bezanilla and Perozo, 2003).

Disease-causing mutations in neuronal KCNQ2/3 channels locate to the C-terminal domain, the pore domain, and the voltage-sensing domain (Maljevic and Lerche, 2014). Among the most severe disease-causing mutations in neuronal KCNQ channels are those affecting the S4 segment (Maljevic and Lerche, 2014; Millichap et al., 2016). In particular, mutations that neutralize the second positively charged arginine residue (R2) in S4 from KCNQ channels cause drastic functional channel defects (Panaghie and Abbott, 2007; Miceli et al., 2008, 2012, 2015; Bartos et al., 2011). Thus, it has been hypothesized that mutations

Division of Endocrinology, Diabetes, and Metabolism, Department of Medicine, Miller School of Medicine, University of Miami, Miami, FL.

Correspondence to Rene Barro-Soria: rbarro@miami.edu.

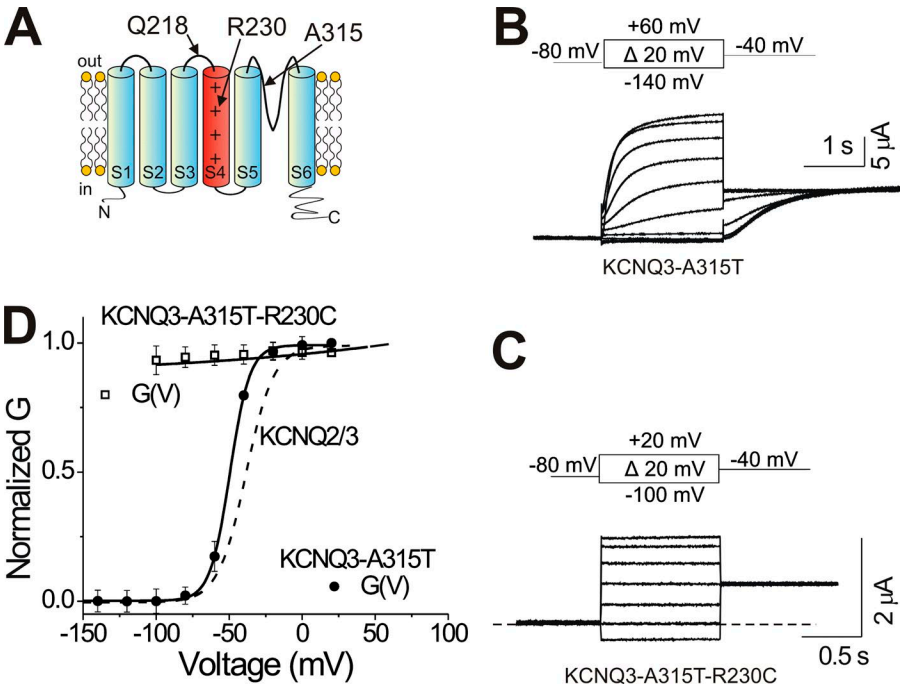


Figure 1. **R230C alters the voltage dependence and kinetics of KCNQ3 channels. (A)** Cartoon of KCNQ3 channel representing residues mutated in this study. **(B and C)** Representative current traces from KCNQ3-A315T (B) and KCNQ3-A315T-R230C (C) channels for the indicated voltage protocols. Dashed line represents zero current. **(D)** Extrapolated tail conductances from B and C were normalized ($G(V)$, see Materials and methods) and plotted versus test voltages (WT: KCNQ3-A315T circles; KCNQ3-A315T-R230C squares; means ± SEM, $n$ = 7–13). For comparison, the tail conductance (dashed line) fit of heteromeric KCNQ2/KCNQ3 channel is shown. Lines represent the fitted theoretical voltage dependencies (Eqs. 1 and 2).

that neutralize R2 in KCNQ2 channels stabilize the activated state configuration of the voltage-sensing domain (Miceli et al., 2012, 2015) and, thereby, cause time- and voltage-independent currents. Other possibilities include that neutralization of R2 could impair the coupling between the S4 and the gate, thereby keeping the gate always open independently of S4 movement, or could shift the open/closed transition of the gate to negative potentials, making the channel constitutively conducting in the physiological voltage range.

Here, I tested these alternatives by simultaneously tracking changes in S4 movement and gate opening, using voltage clamp fluorometry (VCF) to understand the mechanism by which the epileptic encephalopathy–causing mutation KCNQ3-R230C impairs channel function. To better understand the impact that alterations in size and charge of R230C have on the movement of S4 and, ultimately, function, I also combine (a) two-electrode voltage clamp with cysteine modification using methanethiosulfonate ethylammonium (MTSEA) and (b) introduction of a variety of natural amino acids and the arginine analogue citrulline (unnatural) into the S4 of KCNQ3 channel. In summary, KCNQ3-R230C channel is hard to close, but it is capable of being closed at extreme negative voltages, which suggests that compounds that shift the voltage dependence of S4 activation to more positive voltages would promote gate closing and have therapeutic potential.

## Materials and methods

### Molecular biology

Mutations were introduced into human KCNQ3 (a gift from Dr. Harley T. Kurata, University of Alberta, Alberta, Canada) using the Quikchange site-directed mutagenesis kit (Qiagen) and fully sequenced to ensure incorporation of intended mutations and the absence of unwanted mutations (sequencing by Genewiz). Complementary RNA (cRNA) was transcribed in vitro using the mMessage mMachine T7 RNA Transcription Kit (Ambion).

### Electrophysiology

Two-electrode voltage clamp (TEVC) and voltage clamp fluorometry (VCF) experiments were performed as previously reported (Osteen et al., 2012; Barro-Soria et al., 2014). In brief, aliquots of 50 ng RNA coding for KCNQ3 or the KCNQ3 variant RNA were injected into *Xenopus laevis* oocytes. For VCF experiments, 2–5 d after injection, oocytes were labeled for 30 min with 100 µM Alexa Fluor 488 5-maleimide (Molecular Probes) in high [$K^+$]-ND96 solution (98 mM KCl, 1.8 mM $CaCl_2$, 1 mM $MgCl_2$, 5 mM HEPES, pH 7.5, with NaOH) at 4°C. Labeled oocytes were kept on ice to prevent internalization of labeled channels. For TEVC and VCF recordings, oocytes were placed into a recording chamber animal pole "up" in nominally $Ca^{2+}$-free solution (96 mM NaCl, 2 mM KCl, 2.8 mM $MgCl_2$, 5 mM HEPES, pH 7.5, with NaOH). 100 µM $LaCl_3$ was added to the batch solution to block endogenous hyperpolarization-activated currents. At this concentration, $La^{3+}$ did not affect $G(V)$ or $F(V)$ curves from KCNQ3. I assayed cysteine modification using the membrane-permeant thiol reagents MTS EA and MTSET (1 mM and 10 mM, respectively; Toronto Research Chemicals) with bath perfusion of oocytes under TEVC.

Electrical measurements were performed in the TEVC configuration using a Dagan CA-1B amplifier, low-pass filtered at 1 kHz, and sampled at 5 kHz (or for VCF an OC-725C oocyte clamp; Warner Instruments). Microelectrodes were pulled to resistances from 0.3 to 0.5 MΩ when filled with 3 M KCl. Voltage clamp data were digitized at 5 kHz (Axon Digidata 1440A; Molecular Devices) and collected using pClamp 10 (Axon Instruments).

Fluorescence recordings were performed using an Olympus BX51WI upright microscope. Light was focused on the top of the oocyte through a ×20 water-immersion objective (numerical aperture: 1.0, working distance: 2 mm) after being passed

through an Oregon green filter cube (41026; Chroma). Fluorescence signals were focused on a photodiode and amplified with an Axopatch 200B patch clamp amplifier (Axon Instruments). Fluorescence signals were low-pass Bessell-filtered (Frequency Devices) at 100–200 Hz, digitized at 1 kHz, and recorded using pClamp 10.

### Data analysis

To determine the ionic conductance established by a given test voltage, a test voltage pulse was followed by a step to the fixed voltage of −40 mV, and current was recorded following the step. To estimate the conductance $g(V)$ activated at the end of the test pulse to voltage $V$, the current flowing after the hook was exponentially extrapolated to the time of the step and divided by the offset between −40 mV and the reversal potential.

The conductance $g(V)$ associated with different test voltages $V$ in a given experiment was fitted by the relation

$$g(V) = A1 + (A2 - A1)/1 + \exp[-ze(V - V_{1/2})/(k_B T)], \quad (1)$$

where $A1$ and $A2$ are conductances that would be approached at extreme negative or positive voltages, respectively, $V_{1/2}$ is the voltage at which the conductance is $(A1 + A2)/2$, and $z$ is an apparent valence describing the voltage sensitivity of activation ($e$ is the electron charge, $k_B$ the Boltzmann constant, and $T$ the absolute temperature). In my experiments, $A2$ is the maximal conductance activated under extreme depolarization, and $A1$ is the constitutive conductance already present at extreme hyperpolarization. $A1/A2$ is the fraction of conductance that is constitutively activated (which is exceedingly small in WT KCNQ3). Because of the generally different numbers of expressed channels in different oocytes, I compared normalized conductance, $G(V)$ as follows:

$$G(V) = g(V)/A2. \quad (2)$$

Fluorescence signals were corrected for bleaching and time-averaged over 10–40-ms intervals for analysis. The voltage dependence of fluorescence $f(V)$ was analyzed and normalized ($F(V)$) using relations analogous to those for conductance (Eqs. 1 and 2).

To estimate the effect of R230-mutations (mut) relative to the wild type (WT) on Gibbs energy, the following relation was used:

$$\Delta\Delta G_0 = \Delta(zFV_{1/2}) = -F(z^{WT}V_{1/2}{}^{WT} - z^{mut}V_{1/2}{}^{mut}), \quad (3)$$

where $z$ is the gating charge of each channel deduced from the slope ($\kappa$) of the Boltzmann fits according to $z = 25/\kappa$, $\Delta V_{1/2}$ is the mutation (mut)-induced shift in the $V_{1/2}$ values—relative to WT—from the Boltzmann fits, and $F$ is Faraday's constant (Monks et al., 1999; Li-Smerin and Swartz, 2001; DeCaen et al., 2008). This analysis assumes a two-state model; hence it underestimates the $z$ value (Chowdhury and Chanda, 2012). The calculated $\Delta\Delta G_0$ should therefore be seen as an approximation.

### Encoding of citrulline into KCNQ3-R230 in *X. laevis* oocytes

Synthesis of citrulline-pdCpA and its ligation onto synthetic pyrrolysine tRNA (*PylT*) to generate *PylT*-Cit have recently been described in detail (Infield et al., 2018a). *PylT* was used for delivery because it is highly orthogonal in *Xenopus* oocytes (Infield et al., 2018b). Oocytes were injected with a mixture of 80 ng UAG-bearing cRNA and 80 ng Pyl-Cit tRNA. In parallel, the cRNA was injected with full-length (pdCpA ligated) *PylT* (*PylT*-CA) as a negative control. Lack of significant currents arising from the *PylT*-CA–injected condition serves as evidence that the currents in *PylT*-Cit–injected oocytes result from successful encoding of citrulline at the UAG site introduced into the KCNQ3 channels.

### Statistics

All experiments were repeated four or more times from at least seven batches of oocytes. Pairwise comparisons were achieved using Student's *t* test, and multiple comparisons were performed using one-way ANOVA with Tukey's test. Data are represented as means ± SEM, and $n$ represents the number of experiments.

## Results

### KCNQ3-R230C shifts S4 movement and activating gating to very negative voltages

The $K^+$ channels underlying the M current of neurons are formed as heterotetramers of the KCNQ2 and KCNQ3 polypeptides. The epilepsy-causing mutation of interest, R230C, is located in the voltage sensor (S4) segment of KCNQ3 (Fig. 1 A). A conformation in which effects of that mutant could be studied without ambiguities due to subunit composition would be a homomeric channel formed by KCNQ3. However, the KCNQ3 homomeric channel is nonfunctional in cellular expression systems because of a failure of membrane insertion (Etxeberria et al., 2004; Zaika et al., 2008; Gómez-Posada et al., 2010). The mutant A315T (Fig. 1 A), however, produced detectable $K^+$ currents (Fig. 1 B; Zaika et al., 2008) that were half-activated at the voltage $V_{1/2} = -46.5 \pm 3$ mV ($n = 13$; Fig. 1 D), similar to KCNQ2/3 heterotetramers (Fig. 1 D, dashed line, and Fig. S1, A and C). Here, I used in all constructs the homotetramer formed by KCNQ3-A315T as a reference for studying mutations in the 230 position.

To track S4 movement, I introduced a second mutation, Q218C, to attach the fluorophore Alexa Fluor 488 5-maleimide to a position near the extracellular end of the S4 segment (Kim et al., 2017). The labeled KCNQ3-A315T-Q218C channels showed functional properties similar to those of KCNQ3-A315T channels. For example, KCNQ3-A315T-Q218C activated with a voltage dependence that was only slightly shallower and mildly right-shifted compared with KCNQ3-A315T (Fig. S2, A and B, compare black solid and dashed lines).

The mutation R230C of KCNQ3 has been linked to epileptic encephalopathy (Rauch et al., 2012; Allen et al., 2013). KCNQ3-A315T-R230C channels expressed in *Xenopus* oocytes appeared to be constitutively activated at voltages between −80 and +20 mV (Fig. 1, C and D). To further study the effect of mutation R230C on activation gating, I extended the range of voltage (−200 and +20 mV) and simultaneously monitored gate opening (by ionic current) and S4 movement (by fluorescence) using VCF (Barro-Soria et al., 2014).

The mutant to be tested, KCNQ3-A315T-Q218C-R230C, presented two potential binding sites for the fluorescence probe Alexa Fluor 488 5-maleimide. I therefore assessed potential fluorescence changes due to Alexa Fluor 488 5-maleimide bound to KCNQ3-A315T-R230C channels (and thus to the S4 segment) in

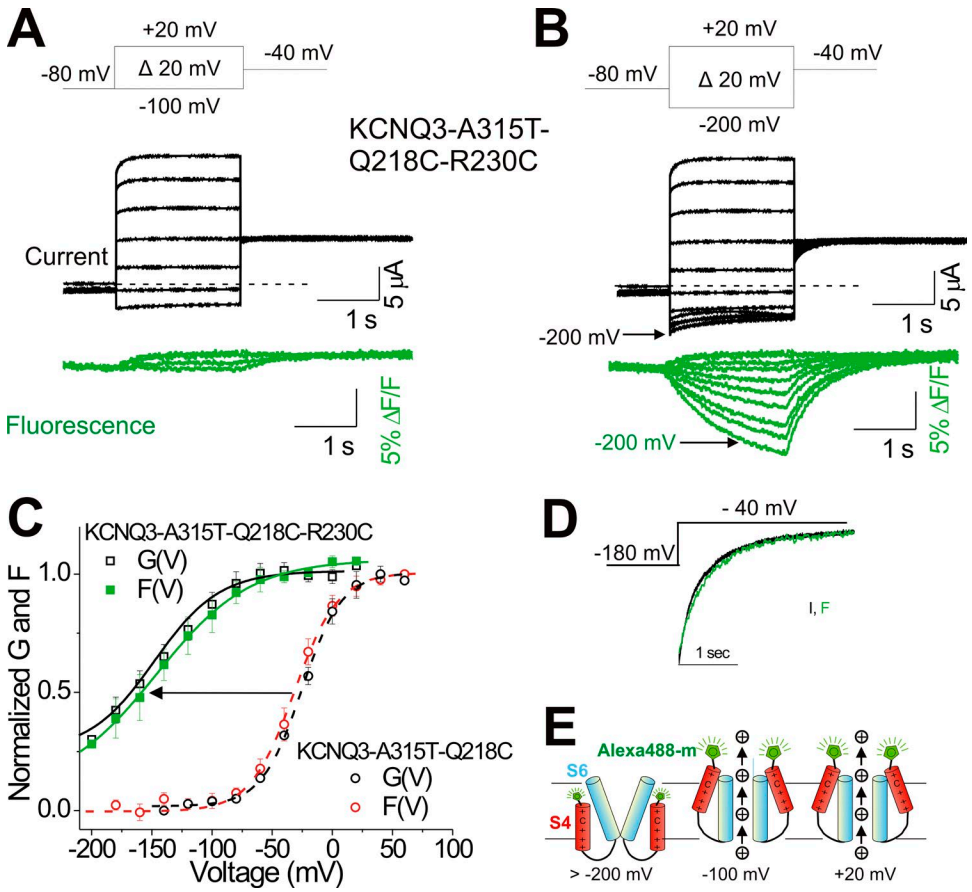


Figure 2. **R230C shifts the voltage sensor movement and gate closing of KCNQ3 channels to very negative voltages. (A and B)** Representative current (black) and fluorescence (green) traces from labeled KCNQ3-A315T-Q218C bearing R230C mutation for the indicated voltage protocols. In response to voltage steps more negative than −100 mV, R230C channels started to close and reopen when stepped back to −40 mV. Dashed lines represent zero current. **(C)** Extrapolated tail conductance (black) and fluorescence (green) from B were normalized (see Materials and methods) and plotted versus test voltages ($G(V)$ and $F(V)$ of KCNQ3-A315T-Q218C-R230C, black and green squares, respectively; means ± SEM, $n$ = 9). The tail conductance (black) and fluorescence (red) of KCNQ3-A315T-Q218C are shown for comparison. Lines represent the fitted theoretical voltage dependencies (see Materials and methods, Eqs. 1 and 2). **(D)** Comparison of activation kinetics of current (black) and fluorescence (green) signals from KCNQ3-A315T-Q218C-R230C in response to the voltage protocol shown. **(E)** Cartoon representing a model of KCNQ3-A315T-Q218C-R230C channel gating where the equilibrium of the S4 movement is shifted to very negative voltages so that at −100 mV, S4 is in the activated position, allowing channel opening. S4 (red), S6 (blue), and Alexa Fluor 488 (green). For simplicity, only two of the four subunits in the tetrameric channel are shown.

response to voltages. No changes were observed with the probe Alexa Fluor 488 5-maleimide (Fig. S2 C), and the ionic currents were like those with unmodified KCNQ3-A315T-R230C channels. I conclude that this probe does not attach to R230C, so that fluorescence changes reported by a probe at Q218C are not obscured by a second attached probe in R230C mutant channels.

Using voltage clamp fluorometry, I observed that over the physiological voltage range (from −100 to +20 mV) the KCNQ3-A315T-Q218C-R230C channels were constitutively open and exhibited very small changes in fluorescence, as if their S4 segments and open gates were locked in place (Fig. 2 A). In contrast, when test voltages between −100 and −200 mV were applied, the fluorescence signal decreased with hyperpolarization (Fig. 2 B, green), as if S4 segments had moved inward (see cartoon in Fig. 2 E). The fluorescence signal increased after the test pulse (Fig. 2 B, green), indicating that the voltage sensors moved from a resting position at approximately −200 mV to an activated position at approximately −100 mV. Simultaneously, I assess the ionic conductance by applying hyperpolarizing voltage test pulses followed by a step to the fixed voltage of −40 mV (Fig. 2 B, black). This step produced relaxations of $K^+$ current, indicating that at the end of the hyperpolarizing test pulse, the $K^+$ conductance was smaller than the conductance eventually reached at −40 mV. When the relaxations of current and fluorescence after the test pulse were scaled and aligned with respect to their end points, they closely superimposed (Fig. 2 D). Displacements of S4 segments and ionic conduction were strongly correlated in time. Thus, the activation of KCNQ3-A315T-Q218-R230C channel was voltage dependent but shifted to more negative potentials compared with WT KCNQ3-A315T-Q218C (Fig. 2 C).

The steady-state fluorescence/voltage curve, $F(V)$ (reflecting voltage sensor movement), and the steady-state conductance/voltage curve, $G(V)$ (reflecting channel opening), in KCNQ3-A315T-Q218-R230C channels were similarly shifted to negative voltages compared with those of KCNQ3-A315T-Q218C channels ($F(V)$ shifted more than −107.1 ± 4.5 mV and $G(V)$ shifted more than −112 ± 3.3 mV, $n$ = 9; Fig. 2 C, arrow). Together, these correlations in time and voltage dependencies indicate that in both

WT and R230C channels, S4 motion and gate operation appeared to be directly coupled: the R230C mutation did not break this coupling. Moreover, S4 motion and gate opening were possible in both WT and R230C channels: the mutation did not interfere with either part of the gating mechanism. Instead, the R230C mutant appeared to shift the voltage-dependent transitions of these channel components to a hyperpolarized, nonphysiological range. Therefore, R230C channels were constitutively open at physiological voltages (–100 to +20 mV; Fig. 2 E).

### The loss of the positive charge of R230 accounts for most of the leftward shift in the *G*(*V*)

The observed leftward shift in both the *F*(*V*) and *G*(*V*) relations of R230C channels relative to WT might be due to (a) loss of the positive charge of the R2 arginine, (b) reduction in the size of the side chain (e.g., from Arg to Cys), or (c) a combination of both. R230 is the second charged residue of the S4 segment (counting from the extracellular end) and thus is likely to contribute directly to the sensing of membrane voltage in KCNQ3 channel (Fig. 1 A). I tested the mutants R230K, (which replaced the guanidinium moiety of the arginine with the ammonium group of the lysine while reducing the size of the side chain), R230H, and chemical modification of R230C by MTSEA, which extended the cysteine side chain and terminated it with an aminoethyl group (Fig. 3, A and B).

In the charge-conservative R230K mutation, the *G*(*V*) curve was more than 45 mV left shifted compared with WT (R230) channels (KCNQ3-R230K: $GV_{1/2}$ = −95 ± 5, *n* = 9; Fig. 3 C, solid arrow). However, the *G*(*V*) curve of R230K was closer to that of the WT R230 than to that of the mutant R230C (Fig. 3 C, dashed arrow), whereas MTSEA-modified R230C and R230H were less effective substitutes of R230 (Fig. 3 C, maroon and green lines, respectively). One possible reason for the lower rescuing effect of MTSEA and R230H is that these residues may not be completely protonated and therefore not completely charged. All three "charged substitutes" of arginine, more prominent in the case of lysine, tended to suppress residual activation at the negative end of the tested voltage range (Fig. 3 C, gray arrow). VCF showed that in the charge-conservative R230K mutation (KCNQ3-A315T-Q218C-R230K), the *F*(*V*) curve closely superimposed the *G*(*V*) curve, and both relations more closely resembled that of the WT KCNQ3-A315T-Q218C in that the S4 movement and channel closing were shifted toward more positive voltages compared with the mutant R230C (KCNQ3-A315T-Q218C-R230K: $GV_{1/2}$ = −88 ± 5, *n* = 8, $FV_{1/2}$ = −92 ± 6, *n* = 8 ; Fig. 3, D and E). The time courses of the fluorescence and ionic current in KCNQ3-A315T-Q218C-R230K were also superimposed (Fig. 3 F, blue dashed and solid lines), and these time courses were faster than the WT KCNQ3-A315T-Q218C (Fig. 3 F, compare blue and red traces). Similar to WT and mutated R230C channels, these correlations in time and voltage dependencies of R230K (and also of 230H, Fig. 3 F, green) further supported that S4 and gate motions were directly coupled. These data also suggest that a positive charge at position R2 directly contributes to sense membrane voltage in KCNQ3 channel but smaller side chains (R-to-K, or guanidinium-to-ammonium) destabilize the resting conformation of the S4, hence promoting channel opening.

An attempt to modify KCNQ3-A315T-R230C using methanethiosulfonate ethyltrimethylammonium (MTSET; one positive formal charge) instead of MTSEA produced no detectable change of R230C channel gating, as if extracellular MTSET was unable to react with R230C (Fig. S3, A and B), similar to what Wu et al. (2010) found when extracellular MTSET failed to modify homologous KCNQ1-R2 cysteine mutant channels. In light of the MTS ET result, it appears possible that the observed modification of KCNQ3-R230C by MTSEA reflects a difference in access to position 230 for these two reagents (MTSEA bears no formal charge, whereas MTSET does), and that the functional consequences of modification by MTSEA may involve only partial or no protonation of the MTSEA aminoethyl group. Moreover, MTSEA specifically modified R230C of KCNQ3, since both the kinetics of activation and *G*(*V*) curves in control KCNQ3 and the mutant KCNQ3-R230A channels treated with MTSEA were similar (Fig. S3, C–E).

Together, these results indicate that, although preserving the positive charge at R2 in the S4 of KCNQ3 channels largely contributes to restoring effective channel gating, it is not sufficient to fully recapitulate the WT channel gating properties.

### The reduction of the side chain size at position 230 contributes to the leftward shift in the *G*(*V*)

Because there is a clear difference in the activation characteristics of R230 and R230K, charge itself is not the sole determinant of function at position 230. To examine the effect of modifying the side chain of R230, I used a nonsense suppression technique to encode the noncanonical amino acid citrulline, an uncharged arginine analogue that retains most of the architecture (volume) of the guanidinium group of arginine (Fig. 4 A). Citrulline is not naturally encoded, albeit posttranslational deimination of arginine residues occurs (György et al., 2006). I introduced citrulline into KCNQ3-R230 channels using in vitro acylated tRNAs (Fig. 4 B), as previously reported (Infield et al., 2018a). Coinjection of citrulline-acylated pyrrolysine tRNA with cRNA of KCNQ3 channels bearing the amber UAG stop codon at 230 rendered voltage-activated potassium currents, which demonstrates successful encoding of citrulline (R230Cit; Fig. 4, B and C, inset trace). As a control, I coinjected (in the same batch of oocytes, the same day and using the same experimental conditions as above) KCNQ3-R230UAG or Shaker-R362UAG (R1UAG) cRNA with nonacylated, full-length (pdCpA-ligated) pyrrolysine tRNA (pyl-tRNA) and Shaker-R1UAG cRNA with Pyl-citrulline (Fig. S4). In the absence of the tethered amino acid, the current was negligible (Fig. S4, A and B), reflective of the orthogonality of this tRNA species in the *Xenopus* oocyte. However, co-injection of Shaker-R1UAG cRNA with Pyl-citrulline rendered robust voltage-activated potassium currents (Fig. S4, C and D), as previously reported (Infield et al., 2018a), thus validating the approach used here.

The *G*(*V*) curve of mutant R230Cit was shifted to negative voltages compared with WT KCNQ3 channels (Fig. 4 C, red circles and red horizontal arrow). Also, the ionic current at −200 mV was significantly reduced compared with KCNQ3-R230C (Fig. 4 C, vertical red arrow). The difference between Arg-to-Cit substitution (which retains most of the Arg side chain's steric

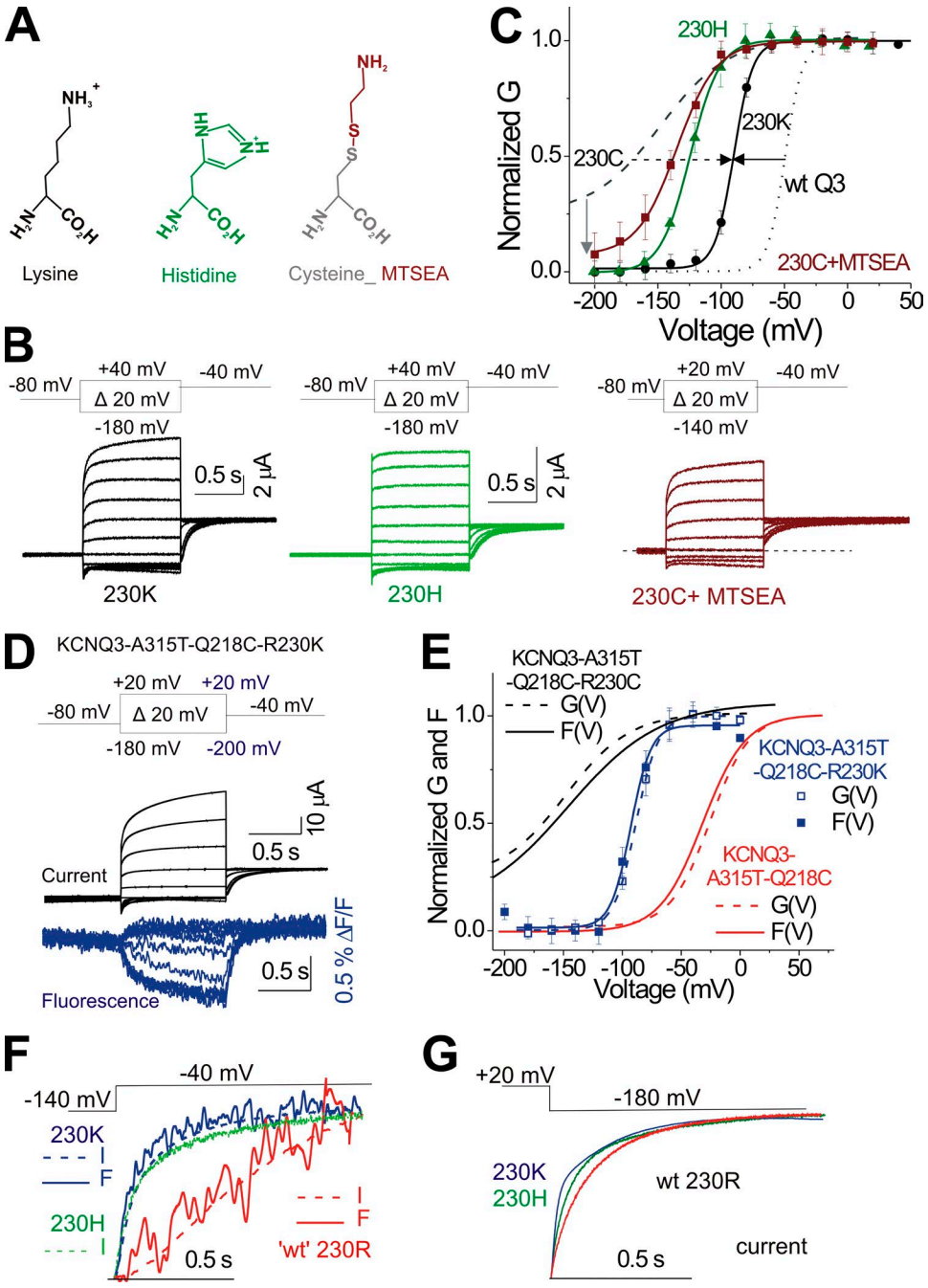


Figure 3. **The loss of the positive charge of R230 accounts for most of the leftward shift in the *G*(*V*). (A)** Structure of lysine, histidine, and a modified cysteine by the thiol reagent MTSEA. **(B)** Representative current traces from KCNQ3-A315T-R230K (black), KCNQ3-A315T-R230H (green), and KCNQ3-A315T-R230C after application of MTSEA (1 mM; maroon) for the indicated voltage protocols. External MTSEA was applied by stepping 15 times to +20 mV for 5 s from a holding voltage of −80 mV and then washed away for 15 s before the indicated voltage protocol was applied. Dotted line represents zero current. **(C)** Extrapolated tail conductances from B were normalized (*G*(*V*), see Materials and methods) and plotted versus test voltages (means ± SEM; $n = 8–9$). Normalized *G*(*V*) of KCNQ3-A315T (WT Q3, dotted line) and KCNQ3-A315T-R230C (dashed line) are shown for comparison. **(D)** Representative current (black) and fluorescence (blue) traces from labeled KCNQ3-A315T-Q218C-R230K for the indicated voltage protocol. **(E)** Extrapolated tail conductance and fluorescence from D were normalized (see Materials and methods) and plotted versus test voltages (*G*(*V*), open squares), and *F*(*V*), filled blue squares) of KCNQ3-A315T-Q218C-R230K (means ± SEM, $n = 10$). For comparison, the tail conductance (dashed lines) and fluorescence (solid lines) fits of KCNQ3-A315T-Q218C-R230C (black) and WT KCNQ3-A315T-Q218C (red), respectively, are shown. Lines represent the fitted theoretical voltage dependencies (see Materials and methods, Eqs. 1 and 2). **(F)** Comparison of the kinetics of ionic current (dashed lines) and fluorescence (solid lines) signals from KCNQ3-A315T-Q218C-R230K (blue) and WT KCNQ3-A315T-Q218C (red), respectively, in response to the voltage protocol. The time course of ionic current of KCNQ3-A315T-R230H (green) is also shown for comparison. **(G)** Comparison of deactivation kinetics of ionic current from KCNQ3-A315T-Q218C-R230K (blue), KCNQ3-A315T-Q218C-R230H (green), and WT KCNQ3-A315T-Q218C (red), respectively, in response to the voltage protocol. The same color code for the different KCNQ3 bearing R230x amino acid substitutions is shown throughout the figure.

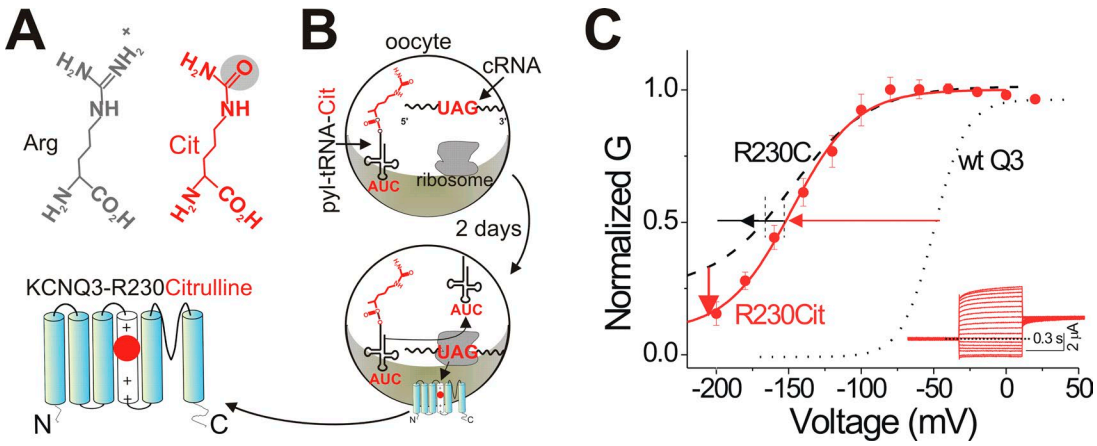


Figure 4. **Encoding of the noncanonical amino acid citrulline quantifies the importance of a positive charge in an otherwise minimally modified side chain at position 230. (A)** Structure of arginine and citrulline. **(B)** Cartoon representing encoding of citrulline into KCNQ3-R230 channels. Co-injection of pyrrolysine tRNA-citrulline with KCNQ3 cRNA containing the site-directed stop codon UAG (nonsense codon) at 230 into *Xenopus* oocytes (top panel). After 2 d of expression, citrulline (red) was incorporated into KCNQ3 channels at position 230 (bottom panel and left zoom in cartoon). **(C)** Extrapolated tail conductance from KCNQ3-A315T-R230Citrulline (red inset) was normalized (see Materials and methods) and plotted versus test voltages ($G(V)$, red solid line; means ± SEM; $n$ = 7). Normalized $G(V)$ of KCNQ3-A315T (WT Q3, dotted black line) and KCNQ3-A315T-R230C (R230C, solid black line) are shown for comparison. Lines represent the fitted theoretical voltage dependencies (see Materials and methods, Eqs. 1 and 2). Inset shows a representative current trace from KCNQ3-R230Citrulline (red). Dotted line represents zero current. Cells were held at −80 mV and stepped to potentials between −160 mV and +60 mV in 10-mV intervals for 0.5 s, followed by a step to −40 mV to record tail currents.

properties) quantifies the importance of a positive charge in an otherwise minimally modified side chain at position 230.

To examine the effect of side chain size of R230 on channel activation, I introduce three different uncharged amino acids at position 230 (A, Q, and W) and measure the ionic currents (Fig. 5 A). The substitutions R230A, R230Q, and R230W (Fig. 5, A and B) produce graded variations of activation characteristics about those already described for (unmodified) R230C. In general, all KCNQ3-230x substitutions (A, Q, and W) left shift the steady-state conductance/voltage relation $G(V)$ compared with WT KCNQ3 channels and reduce the activation slope, which results in varying degrees of activation at the most negative tested voltage, −200 mV (Fig. 5 B). Consequently, the effectiveness of hyperpolarization in deactivating these mutant channels was related to side chain size (Fig. 5 C). Uncharged bulkier side chains appeared more effective in deactivating the channel (Fig. 5 C). The R230W substitution rescued deactivation to extents similar to that of the charged substitution created by reaction of R230C with MTSEA (compare Fig. 3 C and Fig. 5 B). This tendency might also be reflected in the greater effectiveness of WT 230R compared with R230K: both charged residues differed in that the guanidinium moiety of the arginine was slightly larger than the ammonium group of the lysine (Fig. 3 C). Therefore, the difference between R-to-K substitution, which retains the positive charge, quantifies the importance of the guanidinium steric properties at position 230 for normal channel gating (Fig. 3, C and E).

I also aimed to correct for the difference in slope to better compare the functional effect of $G(V)$ shifts on these mutants by calculating changes in Gibbs energy for channel opening ($\Delta\Delta G_0$; Monks et al., 1999; Li-Smerin and Swartz, 2001; DeCaen et al., 2008). However, because the $G(V)$ curves in the R230x substitutions (A, C, Q, and W) do not saturate at negative voltages and/or show various constitutive currents at strong negative voltages, both the $V_{1/2}$ and the activation slopes might not be accurately estimated. I therefore calculated the Gibbs energy only for charged residues R230K and R230H and set a cutoff value of 1 kcal/mol for significant perturbation (Labro et al., 2011). Thus, compared with WT R230R, the R230K and R230H substitutions significantly reduced the energy required to open the channel by 3.8 and 3.9 kcal/mol, respectively (Table 1), as if reducing the size of the side chain would promote stabilization of the channel in an activated open state (or destabilization of the channel closed state). Together, these results suggest that the reduction of the side chain at position 230 alters normal KCNQ3 channel gating, and that bulkier side chains at this position help to restore WT channel function (Fig. 5, B and C).

## Discussion

I investigated the role of residue 230 (R2) in the voltage sensor of homomeric KCNQ3 channels. The mutant R230C renders the channel open throughout the physiological membrane voltage range and has been implicated in epileptic diseases (Miceli et al., 2012, 2015). Mechanisms that could link this functional mutation in neuronal channels to epilepsy have been discussed (Miceli et al., 2015; Niday and Tzingounis, 2018). For example, KCNQ-associated gain-of-function mutations in inhibitory neurons may decrease inhibitory activity, thereby increasing action potential activity in the excitatory pyramidal neurons with which the inhibitory neurons synapse (Miceli et al., 2015). Here, I further investigated how substitution of arginine 230 by cysteine alters channel activation and used a variety of other substitutions to determine side-chain properties that are important for normal or altered activation.

Using VCF, I found that the epilepsy-causing mutation R230C shifted the voltage dependence of S4 movement and channel clos-

Table 1. **Effect of R230x mutations on the S4 of KCNQ3 channel.**

| | *n* | κ (mV) | *z*(*e*) | $V_{1/2}$ (mV) | $\Delta V_{1/2}$ (mV) | $\Delta\Delta G_0$ (kcal/mol) |
|---|---|---|---|---|---|---|
| WT R230R | 13 | 6.8 | 3.7 | −46.5 ± 3.0 | | |
| R230K | 9 | 7.5 | 3.3 | −95.0 ± 5.1 | 48.5 ± 2.2 | −3.8 ± 0.5 |
| R230H | 8 | 11.7 | 2.1 | −124.6 ± 6.3 | 78.1 ± 2.9 | −3.9 ± 0.6 |

Summary of $V_{1/2}$, $\Delta V_{1/2}$, and $\Delta\Delta G_0$ for WT KCNQ3, KCNQ3-R230K, and KCNQ3-R230H substitutions. $V_{1/2}$ is the midpoint of activation, *z* is the valence describing the voltage sensitivity of activation, and κ is the slope of the activation curve fitted with the Boltzmann Eq. 1 (see Materials and methods). $\Delta G_0$ represents the Gibbs free energy of activation at 0 mV. $\Delta\Delta G_0$ is calculated as $[-F(z^{wt}V_{1/2}{}^{wt} - z^{mut}V_{1/2}{}^{mut})]$ and is expressed in kcal/mol. Values are means ± SEM; *n* represents the number of cells analyzed.

ing toward strongly negative voltages. The S4 and gate remained in their activated states at physiological voltages but returned to resting states at hyperpolarizing voltages in the range −80 to −200 mV. In R230K and R230C mutants, the time courses and voltage dependences of fluorescence and ionic current strongly correlated, suggesting that S4 movement and channel opening are directly coupled, as also reported for WT KCNQ3 channels (Kim et al., 2017). This coupling is different from that of KCNQ4 channels, in which the S4 movement and ionic current seem to be "poorly coupled" (Miceli et al., 2012). Measurements of gating current of KCNQ4 showed that the S4 segment moves much faster than the rate of activation revealed by ionic currents, as if S4-charge movement is not directly coupled to opening or closing of KCNQ4 channels (Miceli et al., 2012).

The mutation R230C eliminates the second positive charge (R2) of the S4 transmembrane segment (counted from the extracellular side). Because residue 233 (R3) of KCNQ3 is also uncharged (R3 of all KCNQ1–5 is a Q), a gap of two uncharged positions interrupts the regular chain of charged residues that is characteristic of the S4 segments of many other voltage-dependent channels, such as Shaker. The R2 + R3 gap implies that conserved negative charges on the S2 and S3 transmembrane segments cannot interact with positive S4 charges when the S4 segment is in its resting position (inward), which is associated with the closure of channel gate. I show here that R230K—and with weaker effect, R230H—support, but do not fully rescue, channel closure. Indeed, it has been shown that arginine and lysine form ionizable salt bridges by hydrogen bonding and/or electrostatic charge–charge ionic interactions (Riordan et al., 1977; Borders et al., 1994). Compared with the smaller amino group of the lysine side chain that can form only two hydrogen bonds, arginine can coordinate up to five hydrogen bonds with acidic residues owing to the presence of the larger guanidinium group (Borders et al., 1994). Therefore, it seems that in the R230K mutation, for instance, the loss of at least three hydrogen bonds, caused by the loss of the guanidinium group, or reduced volume contribute to the observed left-shifted channel closure.

By comparing the functional properties of substitutions of R230 with neutral amino acids, I found that the increase in the shape/volume at this position helped stabilize the channel in a deactivated closed state (or helped destabilize the channel-activated conformation). The uncharged close structural analogue of

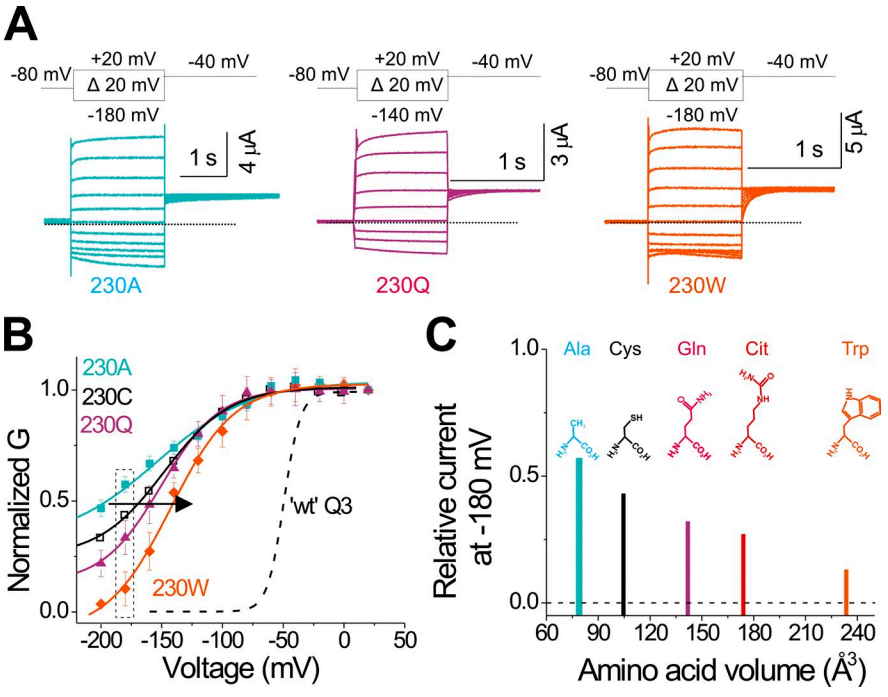


Figure 5. **The reduction of the side chain size at position 230 contributes to the leftward shift in the *G*(*V*). (A)** Representative current traces from KCNQ3-A315T-R230A (light blue), KCNQ3-A315T-R230Q (magenta), and KCNQ3-A315T-R230W (orange) for the indicated voltage protocol. **(B)** Extrapolated tail conductances from R230x mutations from A were normalized (*G*(*V*), see Materials and methods) and plotted versus test voltages (means ± SEM; *n* = 8–11). Lines represent the fitted theoretical voltage dependencies (see Materials and methods, Eqs. 1 and 2). Dashed line represents the *G*(*V*) curve of KCNQ3-A315T (WT Q3) for comparison. Dotted lines represent zero current. **(C)** Relative current at −180 mV from R230x mutations taken from dashed rectangle in B, plotted against amino acid volume in aqueous solution (Zamyatnin, 1972). Dashed line represents the current of WT KCNQ3-A315T-R230R at −180 mV. Structure of the natural amino acids (A, C, Q, and W) and the unnatural amino acid citrulline (Cit), the uncharged close structural analogue of arginine, are shown for comparison. Citrulline volume is estimated from that of arginine. The same color code for the different KCNQ3 bearing R230x amino acid substitutions is shown throughout the figure.

arginine, citrulline, quantified the effect of a missing charge at position 230 that was less than the effect of R230C. Indeed, substitution with uncharged residues at position 230 showed that channel closure moved in a positive direction along the voltage axis in proportion to the number of major atoms in the 230 side chain. The smaller hydrophilic glutamine residue promotes less channel closure than the bulkier aromatic tryptophan residue. It could be that in KCNQ3, bulkier side chains at position 230 (e.g., W over Q for neutral residues or R over K for charged residues) cause a stronger packing of the S4 toward the S5–S6 pore, thereby resulting in a more effective channel closure. Supporting this idea, both 230H and 230K substitutions, compared with the bigger side chain of WT 230R, significantly reduced the Gibbs energy required to open the channel (Table 1), as if smaller residues at position 230 (K and H over R) help stabilize the channel in an activated open state (or destabilize the channel closed state). Moreover, reducing the size of the side chain at position 230 for charged residues (K over R) sped up the time course of both fluorescence (S4 movement) and ionic current (channel opening; Fig. 3 F; and note that the time course of current of 230H was also faster compared with WT, green) with minor changes in channel deactivation kinetics (Fig. 3 G), as if smaller side chain residues destabilize the resting conformation of the S4, hence promoting channel opening.

Electrophysiological studies have shown that among the most severe disease-causing mutations in neuronal KCNQ channels, those affecting the gating charge arginine residues (R1–R6) in the S4 profoundly alter the channel's voltage dependence (*GV*) and the macroscopic ionic current kinetics (Miceli et al., 2008, 2013, 2015). Previous glutamine-scanning mutagenesis study and voltage clamp fluorometry experiments showed that R228Q (R1) in KCNQ1 channels exhibit strong hyperpolarized voltage dependencies of both $G(V)$ and $F(V)$ curves, compared with the WT KCNQ1 channel (Wu et al., 2010; Osteen et al., 2012). Likewise, heterologous expression of the infantile spasm- and encephalopathy-causing mutation R198Q (R1) in KCNQ2 channels showed a negative shift of the $G(V)$ curve (30 mV) and a large fraction of channel open at −80 mV, compared with WT KCNQ2 channels (Millichap et al., 2017). Moreover, Miceli et al. (2015) found that, compared with WT KCNQ2 channels, substituting R201 (R2) by histidine or cysteine causes a strong hyperpolarized $G(V)$ shift and time and voltage independent current, respectively. In disulfide cross-linking experiments, they showed that R201 residue and the negative charged residue D172 in the S3 segment electrostatically interact to stabilize the closed state of KCNQ2 channels (Miceli et al., 2015). This observation led them to conclude that in the mutant R201C, which removes this electrostatic interaction, the S4 segment was likely stabilized in its activated position. Studies from the closely related KCNQ1 and KCNQ4 channels also showed that neutralization mutations at homologous R2 residue lead to constitutively conducting channels (Panaghie and Abbott, 2007; Itoh et al., 2009; Wu et al., 2010; Bartos et al., 2011; Miceli et al., 2012). Interestingly, unlike other R2 neutralization mutations in KCNQ channels, R231C (R2) in KCNQ1 has been reported to show pleiotropic expression. Thus, coexpression of WT KCNQ1 and KCNQ1-R231C subunits showed that the ensembled heteromeric channel had a mixed functional phenotype that has both loss-of-function and gain-of-function properties (Bartos et al., 2011). Similar to heteromeric KCNQ2/KCNQ3 channels bearing the R230C mutation studied here, two independent studies showed that heteromeric KCNQ1/KCNQ1-R231C exhibited a large fraction of constitutive ionic conductance even at strong negative voltages and a marked negative shift of the $G(V)$ curve compared with homomeric WT KCNQ1 (Bartos et al., 2011), as if channels containing two activated voltage sensors have a ∼30% probability of opening (Osteen et al., 2012). By contrast, using a ventricular action potential waveform protocol, Bartos et al. (2011) also showed that cells expressing heteromeric KCNQ1/KCNQ1-R231C channels were able to reduce the fraction of current that remained after repolarization to diastolic potentials, a phenotype consisting with a loss of channel function. This unique sensitivity of R2 to mutations in KCNQ channels seems different from, for example, neutralization mutations affecting charged residues located in the C-terminal portion of S4 within KCNQ channels, which have been shown to decrease the stability of the open state (or increase the stability of the closed state) and the active voltage-sensing domain configuration as shown by the depolarized shift of the $G(V)$ curve (Wu et al., 2010; Miceli et al., 2012). For example, two scanning mutagenesis studies showed that neutralization mutations of R4 and R6 from KCNQ1 channel shifted the $G(V)$ curve to positive voltages (Panaghie and Abbott, 2007; Wu et al., 2010)—the deactivation time constant of R237A (R4) being remarkably slower compared with WT KCNQ1 channels (Panaghie and Abbott, 2007). Similarly, functional studies in KCNQ2 channels revealed that R3Q, R6Q, and R6W substitutions shift the $G(V)$ curve to positive voltages and slow the kinetics of activation, suggesting that neutralization mutations destabilize the open state (Miceli et al., 2008, 2013). In general, it seems that in KCNQ channels, charged residues located in the N-terminal portion of S4 (e.g., R1 and R2) contribute to stabilizing the S4 in its resting (inward) conformation, whereas charged residues in the C-terminal portion of S4 (e.g., R6) stabilize the activated conformation of the S4 (outward), as previously suggested for KCNQ1 channels (Wu et al., 2010). Notably, none of these studies directly measured S4 motion in KCNQ2 or KCNQ3 mutated channels, possibly because of a combination of low expression, few S4 charges and/or slow S4 movements compared with other Kv channels. The VCF and systematic amino acid substitution data shown here offer a mechanistic explanation for how neutralization mutations at R2 of other KCNQ may cause constitutive conducting channels.

This study demonstrates that R230C shifts the voltage dependence of S4 movement and channel opening by more than −100 mV, thereby converting KCNQ3 bearing R230C mutation into a voltage-independent channel in the physiological voltage range. This dramatic change in mutated KCNQ3-R230C channel gating is likely due to a combination of both the reduction of the side chain together with the loss of the positive charge at position 230. Impaired KCNQ3 channel function leads to a defective $I_{KM}$ channel that, in turn, accounts for the neuronal hyperexcitability-related phenotype observed in KCNQ3-R230 mutant channels. Indeed, I found that in heteromeric channels assembled from WT KCNQ2, WT KCNQ3, and KCNQ3-R230C (in a 2:1:1 ratio), the $G(V)$ curve was shifted to negative voltages by >15 mV compared

with heteromeric WT KCNQ2/3 channels (Fig. S1, A–C, arrow). The current also revealed a 1–5% constitutive conductance even at strongly hyperpolarized potentials (Fig. S1, B′ and C, dotted gray rectangle), as if only one R230C subunit would be sufficient to impair full channel closure. The finding that the homomeric 230C of KCNQ3 allows S4 movement but shifts the open/closed transition of the gate to strongly negative potentials provides a mechanistic platform to explain how at resting potentials heteromeric channels bearing even one 230C subunit, as in epileptic phenotypes, conduct more ionic current than WT channels. Thus, neurons from patients bearing the R230C mutation are more hyperpolarized than those of normal individuals owing to more KCNQ-associated potassium conductance (Fig. S1 C). However, because inhibitory neurons have larger input resistance compared with principal neurons (Zemankovics et al., 2010), a leftward shift in the $G(V)$ curve, such as that from heteromeric channels bearing the R230C mutation, would have a larger "silencing" effect in inhibitory neurons than in principal neurons, thereby enhancing excitability in principal neurons with which inhibitory neurons synapse. This suggests that compounds that can right shift the voltage dependence of S4 activation would promote gate closing and have therapeutic potential. This study not only provides mechanistic insights into a better understanding of the molecular basis by which mutations in the $I_{KM}$ channel are linked to epilepsy, but also lays the groundwork for a potential platform for drug development.

## Acknowledgments

I thank Drs. Derek M. Dykxhoorn, H. Peter Larsson, and Wolfgang Nonner for helpful comments on the manuscript. I thank Marta E. Perez for technical assistance in molecular biology and Dr. Harley T. Kurata (University of Alberta, Canada) for the generous gift of the KCNQ3 construct.

I also thank Dr. Christopher A. Ahern for the pyrrolysine tRNA-citrulline, tRNA-pdCpA, and Shaker-R1TAG constructs through National Institutes of Health grant R24NS104617 to Dr. Ahern. This work was supported by a Taking Flight award from Citizens United for Research in Epilepsy (414889) and a National Institutes of Health grant (K01NS096778) to R. Barro-Soria.

The author declares no competing financial interests.

Author contributions: R. Barro-Soria performed voltage clamp, voltage clamp fluorometry, MTS-modification recordings, and molecular biology, analyzed the data, and wrote the manuscript.

Richard W. Aldrich served as editor.

Submitted: 17 August 2018
Accepted: 3 December 2018

## References

Aggarwal, S.K., and R. MacKinnon. 1996. Contribution of the S4 segment to gating charge in the Shaker K+ channel. *Neuron.* 16:1169–1177. https://doi.org/10.1016/S0896-6273(00)80143-9

Allen, A.S., S.F. Berkovic, P. Cossette, N. Delanty, D. Dlugos, E.E. Eichler, M.P. Epstein, T. Glauser, D.B. Goldstein, Y. Han, et al. Epilepsy Phenome/Genome Project. 2013. De novo mutations in epileptic encephalopathies. *Nature.* 501:217–221. https://doi.org/10.1038/nature12439

Barro-Soria, R., S. Rebolledo, S.I. Liin, M.E. Perez, K.J. Sampson, R.S. Kass, and H.P. Larsson. 2014. KCNE1 divides the voltage sensor movement in KCNQ1/KCNE1 channels into two steps. *Nat. Commun.* 5:3750. https://doi.org/10.1038/ncomms4750

Bartos, D.C., S. Duchatelet, D.E. Burgess, D. Klug, I. Denjoy, R. Peat, J.M. Lupoglazoff, V. Fressart, M. Berthet, M.J. Ackerman, et al. 2011. R231C mutation in KCNQ1 causes long QT syndrome type 1 and familial atrial fibrillation. *Heart Rhythm.* 8:48–55. https://doi.org/10.1016/j.hrthm.2010.09.010

Bezanilla, F., and E. Perozo. 2003. The voltage sensor and the gate in ion channels. *Adv. Protein Chem.* 63:211–241. https://doi.org/10.1016/S0065-3233(03)63009-3

Biervert, C., B.C. Schroeder, C. Kubisch, S.F. Berkovic, P. Propping, T.J. Jentsch, and O.K. Steinlein. 1998. A potassium channel mutation in neonatal human epilepsy. *Science.* 279:403–406. https://doi.org/10.1126/science.279.5349.403

Borders, C.L. Jr., J.A. Broadwater, P.A. Bekeny, J.E. Salmon, A.S. Lee, A.M. Eldridge, and V.B. Pett. 1994. A structural role for arginine in proteins: multiple hydrogen bonds to backbone carbonyl oxygens. *Protein Sci.* 3:541–548. https://doi.org/10.1002/pro.5560030402

Brown, D.A., and P.R. Adams. 1980. Muscarinic suppression of a novel voltage-sensitive K+ current in a vertebrate neurone. *Nature.* 283:673–676. https://doi.org/10.1038/283673a0

Charlier, C., N.A. Singh, S.G. Ryan, T.B. Lewis, B.E. Reus, R.J. Leach, and M. Leppert. 1998. A pore mutation in a novel KQT-like potassium channel gene in an idiopathic epilepsy family. *Nat. Genet.* 18:53–55. https://doi.org/10.1038/ng0198-53

Chowdhury, S., and B. Chanda. 2012. Estimating the voltage-dependent free energy change of ion channels using the median voltage for activation. *J. Gen. Physiol.* 139:3–17. https://doi.org/10.1085/jgp.201110722

DeCaen, P.G., V. Yarov-Yarovoy, Y. Zhao, T. Scheuer, and W.A. Catterall. 2008. Disulfide locking a sodium channel voltage sensor reveals ion pair formation during activation. *Proc. Natl. Acad. Sci. USA.* 105:15142–15147. https://doi.org/10.1073/pnas.0806486105

del Camino, D., and G. Yellen. 2001. Tight steric closure at the intracellular activation gate of a voltage-gated K(+) channel. *Neuron.* 32:649–656. https://doi.org/10.1016/S0896-6273(01)00487-1

Etxeberria, A., I. Santana-Castro, M.P. Regalado, P. Aivar, and A. Villarroel. 2004. Three mechanisms underlie KCNQ2/3 heteromeric potassium M-channel potentiation. *J. Neurosci.* 24:9146–9152. https://doi.org/10.1523/JNEUROSCI.3194-04.2004

Gómez-Posada, J.C., A. Etxeberría, M. Roura-Ferrer, P. Areso, M. Masin, R.D. Murrell-Lagnado, and A. Villarroel. 2010. A pore residue of the KCNQ3 potassium M-channel subunit controls surface expression. *J. Neurosci.* 30:9316–9323. https://doi.org/10.1523/JNEUROSCI.0851-10.2010

György, B., E. Tóth, E. Tarcsa, A. Falus, and E.I. Buzás. 2006. Citrullination: a posttranslational modification in health and disease. *Int. J. Biochem. Cell Biol.* 38:1662–1677. https://doi.org/10.1016/j.biocel.2006.03.008

Halliwell, J.V., and P.R. Adams. 1982. Voltage-clamp analysis of muscarinic excitation in hippocampal neurons. *Brain Res.* 250:71–92. https://doi.org/10.1016/0006-8993(82)90954-4

Infield, D.T., E.E.L. Lee, J.D. Galpin, G.D. Galles, F. Bezanilla, and C.A. Ahern. 2018a. Replacing voltage sensor arginines with citrulline provides mechanistic insight into charge versus shape. *J. Gen. Physiol.* 150:1017–1024.

Infield, D.T., J.D. Lueck, J.D. Galpin, G.D. Galles, and C.A. Ahern. 2018b. Orthogonality of Pyrrolysine tRNA in the Xenopus oocyte. *Sci. Rep.* 8:5166. https://doi.org/10.1038/s41598-018-23201-z

Itoh, H., T. Sakaguchi, W.G. Ding, E. Watanabe, I. Watanabe, Y. Nishio, T. Makiyama, S. Ohno, M. Akao, Y. Higashi, et al. 2009. Latent genetic backgrounds and molecular pathogenesis in drug-induced long-QT syndrome. *Circ Arrhythm Electrophysiol.* 2:511–523. https://doi.org/10.1161/CIRCEP.109.862649

Jentsch, T.J. 2000. Neuronal KCNQ potassium channels: physiology and role in disease. *Nat. Rev. Neurosci.* 1:21–30. https://doi.org/10.1038/35036198

Kato, M., T. Yamagata, M. Kubota, H. Arai, S. Yamashita, T. Nakagawa, T. Fujii, K. Sugai, K. Imai, T. Uster, et al. 2013. Clinical spectrum of early onset epileptic encephalopathies caused by KCNQ2 mutation. *Epilepsia.* 54:1282–1287. https://doi.org/10.1111/epi.12200

Kim, R.Y., S.A. Pless, and H.T. Kurata. 2017. PIP2 mediates functional coupling and pharmacology of neuronal KCNQ channels. *Proc. Natl. Acad. Sci. USA.* 114:E9702–E9711. https://doi.org/10.1073/pnas.1705802114

Labro, A.J., I.R. Boulet, F.S. Choveau, E. Mayeur, T. Bruyns, G. Loussouarn, A.L. Raes, and D.J. Snyders. 2011. The S4-S5 linker of KCNQ1 channels forms

a structural scaffold with the S6 segment controlling gate closure. *J. Biol. Chem.* 286:717–725. https://doi.org/10.1074/jbc.M110.146977

Larsson, H.P., O.S. Baker, D.S. Dhillon, and E.Y. Isacoff. 1996. Transmembrane movement of the shaker K+ channel S4. *Neuron.* 16:387–397. https://doi.org/10.1016/S0896-6273(00)80056-2

Li-Smerin, Y., and K.J. Swartz. 2001. Helical structure of the COOH terminus of S3 and its contribution to the gating modifier toxin receptor in voltage-gated ion channels. *J. Gen. Physiol.* 117:205–218. https://doi.org/10.1085/jgp.117.3.205

Long, S.B., E.B. Campbell, and R. Mackinnon. 2005. Crystal structure of a mammalian voltage-dependent Shaker family K+ channel. *Science.* 309:897–903. https://doi.org/10.1126/science.1116269

Maljevic, S., and H. Lerche. 2014. Potassium channel genes and benign familial neonatal epilepsy. *Prog. Brain Res.* 213:17–53. https://doi.org/10.1016/B978-0-444-63326-2.00002-8

Mannuzzu, L.M., M.M. Moronne, and E.Y. Isacoff. 1996. Direct physical measure of conformational rearrangement underlying potassium channel gating. *Science.* 271:213–216. https://doi.org/10.1126/science.271.5246.213

Miceli, F., M.V. Soldovieri, C.C. Hernandez, M.S. Shapiro, L. Annunziato, and M. Taglialatela. 2008. Gating consequences of charge neutralization of arginine residues in the S4 segment of K(v)7.2, an epilepsy-linked K+ channel subunit. *Biophys. J.* 95:2254–2264. https://doi.org/10.1529/biophysj.107.128371

Miceli, F., E. Vargas, F. Bezanilla, and M. Taglialatela. 2012. Gating currents from Kv7 channels carrying neuronal hyperexcitability mutations in the voltage-sensing domain. *Biophys. J.* 102:1372–1382. https://doi.org/10.1016/j.bpj.2012.02.004

Miceli, F., M.V. Soldovieri, P. Ambrosino, V. Barrese, M. Migliore, M.R. Cilio, and M. Taglialatela. 2013. Genotype-phenotype correlations in neonatal epilepsies caused by mutations in the voltage sensor of K(v)7.2 potassium channel subunits. *Proc. Natl. Acad. Sci. USA.* 110:4386–4391. https://doi.org/10.1073/pnas.1216867110

Miceli, F., M.V. Soldovieri, P. Ambrosino, M. De Maria, M. Migliore, R. Migliore, and M. Taglialatela. 2015. Early-onset epileptic encephalopathy caused by gain-of-function mutations in the voltage sensor of Kv7.2 and Kv7.3 potassium channel subunits. *J. Neurosci.* 35:3782–3793. https://doi.org/10.1523/JNEUROSCI.4423-14.2015

Millichap, J.J., K.L. Park, T. Tsuchida, B. Ben-Zeev, L. Carmant, R. Flamini, N. Joshi, P.M. Levisohn, E. Marsh, S. Nangia, et al. 2016. KCNQ2 encephalopathy: Features, mutational hot spots, and ezogabine treatment of 11 patients. *Neurol. Genet.* 2:e96. https://doi.org/10.1212/NXG.0000000000000096

Millichap, J.J., F. Miceli, M. De Maria, C. Keator, N. Joshi, B. Tran, M.V. Soldovieri, P. Ambrosino, V. Shashi, M.A. Mikati, et al. 2017. Infantile spasms and encephalopathy without preceding neonatal seizures caused by KCNQ2 R198Q, a gain-of-function variant. *Epilepsia.* 58:e10–e15. https://doi.org/10.1111/epi.13601

Monks, S.A., D.J. Needleman, and C. Miller. 1999. Helical structure and packing orientation of the S2 segment in the Shaker K+ channel. *J. Gen. Physiol.* 113:415–423. https://doi.org/10.1085/jgp.113.3.415

Niday, Z., and A.V. Tzingounis. 2018. Potassium Channel Gain of Function in Epilepsy: An Unresolved Paradox. *Neuroscientist.* 24:368–380. https://doi.org/10.1177/1073858418763752

Orhan, G., M. Bock, D. Schepers, E.I. Ilina, S.N. Reichel, H. Löffler, N. Jezutkovic, S. Weckhuysen, S. Mandelstam, A. Suls, et al. 2014. Dominant-negative effects of KCNQ2 mutations are associated with epileptic encephalopathy. *Ann. Neurol.* 75:382–394. https://doi.org/10.1002/ana.24080

Osteen, J.D., C. Gonzalez, K.J. Sampson, V. Iyer, S. Rebolledo, H.P. Larsson, and R.S. Kass. 2010. KCNE1 alters the voltage sensor movements necessary to open the KCNQ1 channel gate. *Proc. Natl. Acad. Sci. USA.* 107:22710–22715. https://doi.org/10.1073/pnas.1016300108

Osteen, J.D., R. Barro-Soria, S. Robey, K.J. Sampson, R.S. Kass, and H.P. Larsson. 2012. Allosteric gating mechanism underlies the flexible gating of KCNQ1 potassium channels. *Proc. Natl. Acad. Sci. USA.* 109:7103–7108. https://doi.org/10.1073/pnas.1201582109

Panaghie, G., and G.W. Abbott. 2007. The role of S4 charges in voltage-dependent and voltage-independent KCNQ1 potassium channel complexes. *J. Gen. Physiol.* 129:121–133.

Rauch, A., D. Wieczorek, E. Graf, T. Wieland, S. Endele, T. Schwarzmayr, B. Albrecht, D. Bartholdi, J. Beygo, N. Di Donato, et al. 2012. Range of genetic mutations associated with severe non-syndromic sporadic intellectual disability: an exome sequencing study. *Lancet.* 380:1674–1682. https://doi.org/10.1016/S0140-6736(12)61480-9

Riordan, J.F., K.D. McElvany, and C.L. Borders Jr. 1977. Arginyl residues: anion recognition sites in enzymes. *Science.* 195:884–886. https://doi.org/10.1126/science.190679

Saitsu, H., M. Kato, A. Koide, T. Goto, T. Fujita, K. Nishiyama, Y. Tsurusaki, H. Doi, N. Miyake, K. Hayasaka, and N. Matsumoto. 2012. Whole exome sequencing identifies KCNQ2 mutations in Ohtahara syndrome. *Ann. Neurol.* 72:298–300. https://doi.org/10.1002/ana.23620

Seoh, S.A., D. Sigg, D.M. Papazian, and F. Bezanilla. 1996. Voltage-sensing residues in the S2 and S4 segments of the Shaker K+ channel. *Neuron.* 16:1159–1167. https://doi.org/10.1016/S0896-6273(00)80142-7

Singh, N.A., C. Charlier, D. Stauffer, B.R. DuPont, R.J. Leach, R. Melis, G.M. Ronen, I. Bjerre, T. Quattlebaum, J.V. Murphy, et al. 1998. A novel potassium channel gene, KCNQ2, is mutated in an inherited epilepsy of newborns. *Nat. Genet.* 18:25–29. https://doi.org/10.1038/ng0198-25

Sun, J., and R. MacKinnon. 2017. Cryo-EM structure of a KCNQ1/CaM complex reveals insights into congenital long QT syndrome. *Cell.* 169:1042–1050.e9.

Wang, H.S., Z. Pan, W. Shi, B.S. Brown, R.S. Wymore, I.S. Cohen, J.E. Dixon, and D. McKinnon. 1998. KCNQ2 and KCNQ3 potassium channel subunits: molecular correlates of the M-channel. *Science.* 282:1890–1893.

Weckhuysen, S., S. Mandelstam, A. Suls, D. Audenaert, T. Deconinck, L.R. Claes, L. Deprez, K. Smets, D. Hristova, I. Yordanova, et al. 2012. KCNQ2 encephalopathy: emerging phenotype of a neonatal epileptic encephalopathy. *Ann. Neurol.* 71:15–25. https://doi.org/10.1002/ana.22644

Weckhuysen, S., V. Ivanovic, R. Hendrickx, R. Van Coster, H. Hjalgrim, R.S. Møller, S. Grønborg, A.S. Schoonjans, B. Ceulemans, S.B. Heavin, et al. KCNQ2 Study Group. 2013. Extending the KCNQ2 encephalopathy spectrum: clinical and neuroimaging findings in 17 patients. *Neurology.* 81:1697–1703. https://doi.org/10.1212/01.wnl.0000435296.72400.a1

Wu, D., H. Pan, K. Delaloye, and J. Cui. 2010. KCNE1 remodels the voltage sensor of Kv7.1 to modulate channel function. *Biophys. J.* 99:3599–3608. https://doi.org/10.1016/j.bpj.2010.10.018

Yang, N., A.L. George Jr., and R. Horn. 1996. Molecular basis of charge movement in voltage-gated sodium channels. *Neuron.* 16:113–122.

Zaika, O., C.C. Hernandez, M. Bal, G.P. Tolstykh, and M.S. Shapiro. 2008. Determinants within the turret and pore-loop domains of KCNQ3 K+ channels governing functional activity. *Biophys. J.* 95:5121–5137. https://doi.org/10.1529/biophysj.108.137604

Zamyatnin, A.A. 1972. Protein volume in solution. *Prog. Biophys. Mol. Biol.* 24:107–123. https://doi.org/10.1016/0079-6107(72)90005-3

Zemankovics, R., S. Káli, O. Paulsen, T.F. Freund, and N. Hájos. 2010. Differences in subthreshold resonance of hippocampal pyramidal cells and interneurons: the role of h-current and passive membrane characteristics. *J. Physiol.* 588:2109–2132. https://doi.org/10.1113/jphysiol.2009.185975